A Buffer Gas Cooled Molecular Beam Apparatus for Chirped Pulse Millimeter Wave Spectroscopy

by

Ethan Avram Klein

Submitted to the Department of Chemistry
in partial fulfillment of the requirements for the degree of

Bachelor of Science in Chemistry

at the

MASSACHUSETTS INSTITUTE OF TECHNOLOGY

June 2015

Signature redacted

Author .....
Department of Chemistry
May 8, 2015

Signature redacted

Certified by .....
Robert W. Field
Haslam & Dewey Professor of Chemistry
Thesis Supervisor

Signature redacted

Accepted by .....
Rick L. Danheiser
Undergraduate Officer, Department of Chemistry

A Buffer Gas Cooled Molecular Beam Apparatus for Chirped Pulse Millimeter Wave Spectroscopy

by

Ethan Avram Klein

Submitted to the Department of Chemistry
on May 8, 2015, in partial fulfillment of the
requirements for the degree of
Bachelor of Science in Chemistry

Abstract

An apparatus that utilizes buffer gas cooling to produce slow atomic (Ba, Ca) and molecular (BaF, CaF) beams is constructed. In-cell temperatures of 20 ± 0.25K are achieved with chamber cooldown times of under two hours. Laser Induced Fluorescence (LIF) spectra of BaF and CaF confirmed thermalization of the molecular beam to the temperature of the buffer gas and additional hydrodynamic cooling to rotational and translational temperatures under 10K. Laser fluence effects on the intensity of barium and calcium ablation were studied and used to optimize laser parameters for maximum ablation of the desired species. A chirped pulse millimeter wave (CP-mmW) setup was combined with the buffer gas cooling apparatus for combined laser and millimeter wave spectroscopy experiments of Rydberg states. LabVIEW programming is used for an internal temperature feedback system, raster scanning of the ablation target, as well as millimeter wave FID signal digital acquisition. Use of the apparatus for chirped pulse microwave spectroscopy of buffer gas cooled beams have led to orders of magnitude improvement in both the resolution and the reduction of time required to record molecular Rydberg spectra.

Thesis Supervisor: Robert W. Field
Title: Haslam & Dewey Professor of Chemistry

Acknowledgments

I would like to thank my research advisor, Prof. Bob Field, for all his guidance and mentorship. This truly has turned out to be the UROP of my dreams.

I would also like to thank my Rydberg groupmates: Dr. Tony Colombo, Dr. Yan Zhou, David Grimes, and Tim Barnum for their patience and completeness in answering all of my questions about spectroscopy and otherwise, as well as for their grace in dealing with my personal eccentricity.

A special shout-out goes to my fellow Field group UROPs: Julia Berk, Bryan Changala, and Catherine Saladrigas for their camaraderie throughout these past three years.

Contents

Chapter 1

Introduction and Theory

In this introduction, the history of and theory behind molecular cooling techniques, millimeter wave spectroscopy, and laser ablation are reviewed. These three concepts are brought together in the experimental apparatus, the construction of which is detailed in Chapter 2.

1.1 Molecular Beam Sources

The review of molecular beam sources presented here relies heavily on the text Methods of Experimental Physics, Volume 3, Part B and the Hutzler et al. buffer gas cooling review published in *Chemical Reviews*. The author refers the reader to those sources for further information on these subjects.

Electronic spectroscopy of molecules is more complicated than that of atoms due to the presence of rovibrational degrees of freedom. The distribution of population into rotationally and vibrationally excited states dilutes the number density in any given quantum state, reducing experimental sensitivity of a selected quantum state [1]. In addition to high rotational and vibrational temperatures, high translational temperatures of the molecule of interest will Doppler broaden the linewidths of any molecular spectrum. In order to limit the effects of these experimental challenges on molecular spectra, both the molecule's internal (i.e. rotational, vibrational) and translational temperatures must be lowered.

A useful experimental tool for studying gas phase molecules is the formation of a molecular beam. During the past century, different experimental techniques for preparation of molecular beams have been used [2] [3]. Beams produced by oven effusion and supersonic expansion have been utilized for decades, but each technique bears its own set of disadvantages. The technique of buffer gas cooling overcomes these former challenges through cooling of both translational and internal degrees of freedom in addition to slowing lab frame translational velocities.

An applicable quantity for characterizing molecular beam flows is the Reynolds number, Re. The Reynolds number is a ratio of the inertial forces in a flow to the viscous forces, and can be expressed by the equation: $Re = \frac{F_{inertial}}{F_{viscous}} = \frac{\rho V L}{\mu}$, where ρ is the fluid density, V is the flow velocity, L is a length scale, and μ is the dynamic viscosity. For effusive beam flow, Re $\lesssim 1$, indicating dominance of viscous forces. For supersonic beam flow, Re $\gtrsim 100$, and the increased number of collisions leads to more fluid-like behavior. Molecular beam flow in beams cooled by a buffer gas can operate in either of these regimes, but typically lie somewhere in between the two [4].

1.1.1 Effusive Beams

In effusive beam sources, vapor of the molecule of interest effuses through an orifice into an external vacuum. In doing so, a relatively slow moving (200-800m/s), but hot (500-2000K) molecular beam is formed. Around the turn of the century, Knudsen put forth the well-known cosine law of molecular effusion: $dQ_0 = \frac{1}{4\pi} n \bar{v} A_s cos(\theta) d\omega$, where Q_0 is the total molecular flux per second, n is the number density in the source, $\bar{v}$ is the average molecular velocity, A_s is the area of the orifice, and ω is the solid angle [5]. This equation states that the effusion rate of molecules through an orifice into a given solid angle is proportional to the cosine of that angle made with respect to the normal of the orifice. From this equation, the beam intensity of an effusive beam, $I_0(\theta)$ can be derived: $I_0(\theta) = \frac{1}{\pi} Q_0 cos(\theta)$. The maximum effusion rate is therefore at the center of the orifice with the FWHM of the angular distribution subtending an angle of 120°. The formation of an effusive beam is reliant on the assumption that the molecular mean free path is much larger than the orifice diameter, resulting in

few collisions in the vicinity of the orifice [6]. If this were not true, the effusive beam formation would be heavily dependent on interactions with surrounding gas molecules and would not be a reliable sample of the Maxwell Boltzmann distribution. It should be noted that although the velocity distributions within the source can be modeled by a Maxwell-Boltzmann distribution ($f_{mb}(v) \propto v^2 e^{-v^2}$), the distribution of molecules leaving an effusive source is shifted toward higher velocities by an extra factor of v in the distribution ($f_e(v) \propto v^3 e^{-v^2}$), as a consequence of Graham's law of effusion [7].

While effusive beams are slow-moving compared to other beam sources (i.e. supersonic jets), they usually have much higher temperatures. Because sufficient vapor pressure of the molecule of interest at the beam operating temperature is required for beam formation, most effusive beams are based on an oven source. Molecules which are gases at room temperature can usually be cooled prior to effusion, as was done in experiments on H_2 effusive beams run at 20K by Code & Ramsey in 1971 [8]. However, for molecules which are solids at room temperature (such as BaF or CaF in these experiments), significant heating is necessary to generate sufficient vapor pressure. These higher molecular temperatures result in large rotational and vibrational partition functions leading to unwanted population of excited rovibronic quantum states as well as Doppler line broadening.

1.1.2 Supersonic Expansion

Supersonically expanded beams reduce the problems of high molecular temperatures through the resultant cooling of an adiabatic, isentropic expansion of the molecular beam. The supersonic regime is fundamentally different from the effusive regime because the assumption that the mean free path of the molecules is smaller than the orifice diameter no longer holds. In fact, the opposite is true. Collisions between the molecules and the carrier gas near the orifice convert their random thermal motion into directed kinetic energy along the centerline of the flow, lowering the beam temperature considerably. The theory of supersonic jets was first proposed by Kantrowitz & Grey in 1950 and achieved experimentally by Becker & Bier in 1954 before achieving widespread adoption motivated by the work of Smalley, Levy, and Wharton in the late

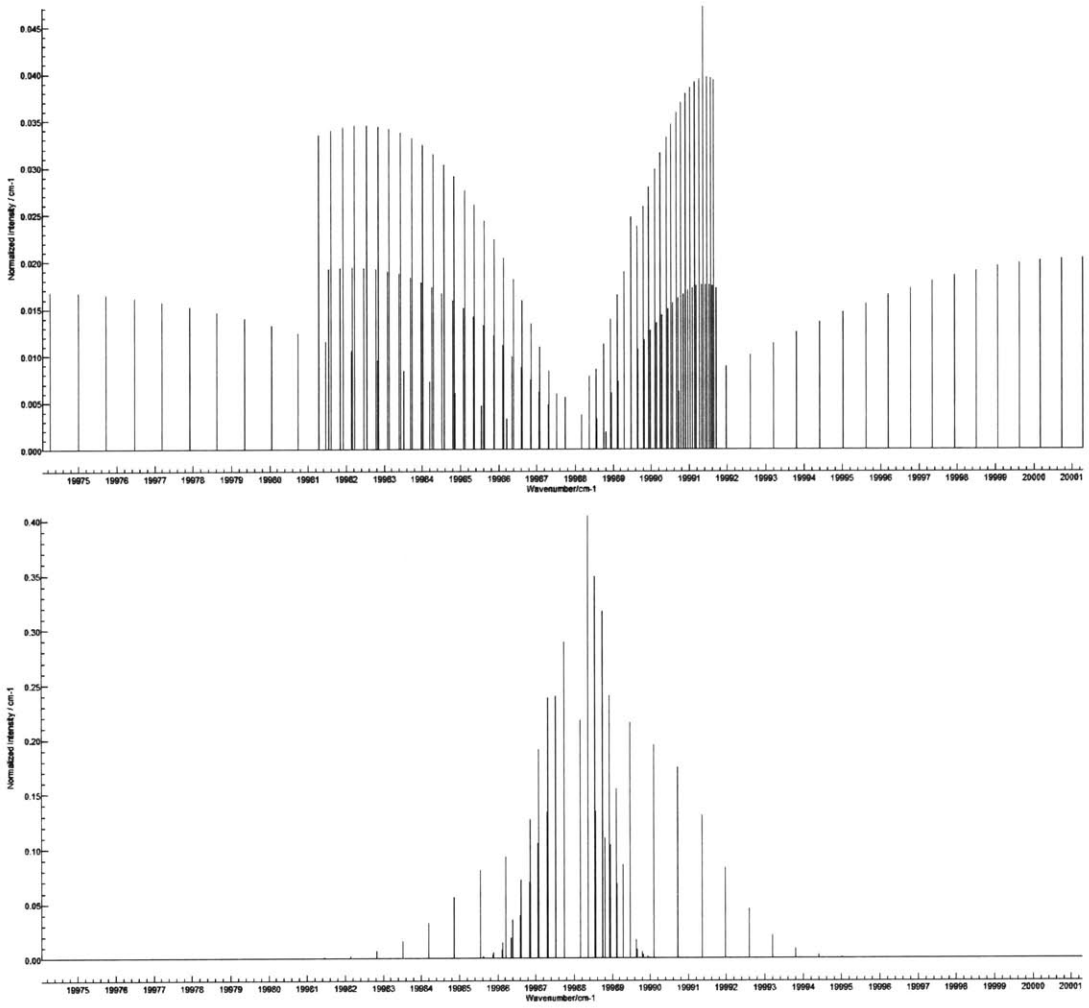

Figure 1-1: A PGopher simulation of the C state of BaF with maximum J=50 for T=300K (top) and T=5K (bottom). Note that the most intense spectral lines at 5K are an order of magnitude more intense than those at 300K.

1960s [9] [10] [11]. Since then, supersonic beam sources have been used successfully in the preparation of internally cooled molecules, radicals, clusters, and molecular complexes.

Utilizing the theory of isentropic expansion, the ratio between the temperature of the molecular beam and the temperature of the molecule in the source chamber can be derived: $\frac{T}{T_0} = \frac{1}{1+\frac{1}{2}(\gamma-1)M^2}$, where M is the Mach number (the ratio of molecular velocity in a medium to the speed of sound in that medium) and $\gamma(= \frac{C_P}{C_V})$ is the adiabatic index. For a monatomic gas (e.g. Ar), T_0=300K, and M=10, the equation gives the translational temperature of the molecular beam as 8.7K. Furthermore, comparing the most probable beam velocities of a supersonic jet with an effusive beam shows that the supersonic beam is a factor of 1.29 times faster for a monatomic gas and 1.53 times faster for a diatomic gas. Despite higher translational velocity, a supersonic molecular beam's distribution of translational velocities is reduced by a factor of $\sqrt{\frac{T_s}{T_e}}$, where T_s is the supersonic beam temperature, and T_e is the effusive beam temperature, compared to an effusive beam. Finally, the intensity gain of using a supersonic beam expansion compared to an effusive beam is defined by the equation $G = \sqrt{\frac{\pi\gamma}{\gamma-1}}\gamma M^2$ which simplifies to $\simeq 4.66M^2$ for large M. For M=5, using a supersonic jet source instead of a effusive source gives an increase of two orders of magnitude in beam intensity [12]. This intensity gain is extremely important in achieving a high enough number density for laser and millimeter wave spectroscopy.

The most significant disadvantage of utilizing a supersonically expanded molecular beam is the high translational velocity of the beam. Having a fast-moving molecular beam in the lab frame means a reduction in possible interrogation time for a spectroscopic experiment. In addition, because the width of the transverse velocity distribution of a molecular beam has been found to be proportional to the Reynolds number of the beam flow, supersonic beams yield larger Doppler broadening than other molecular beams in a transverse experimental configuration [13]. This problem can be surmounted by installing a skimmer to remove only the center of the beam, but it comes at a loss of number of molecules in the beam. In addition to the problem of high velocities, supersonic expansion preferentially cools the molecules translationally

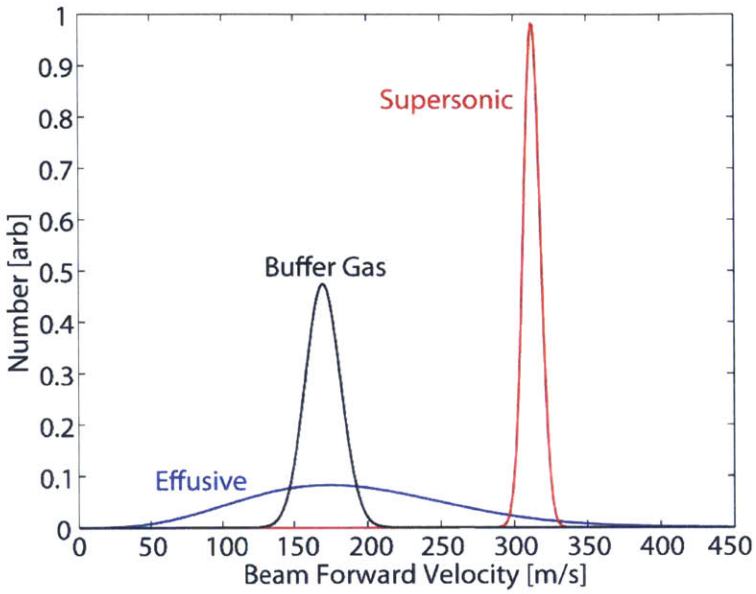

Figure 1-2: The laboratory frame forward velocity distributions of effusive, buffer gas, and supersonic produced beams are shown. Buffer gas cooled beams have wider velocity distributions than supersonic expansions but slower laboratory frame forward velocities. Although not shown here, buffer gas and effusive beams typically have total number densities several orders of magnitude higher than supersonic beams. [4]

($T_{trans} \lesssim T_{rot} << T_{vib}$), leaving some population in excited rovibronic states.

1.1.3 Buffer Gas Cooling

Buffer gas cooling is a technique used to cool a molecule's internal temperature and lower its laboratory frame forward velocity. Buffer gas cooling was first described in a 1984 paper published by Messer & De Lucia describing the pressure-broadening of CO rotational transitions using helium gas to cool the CO [14]. In the 1990s, the use of buffer gas cooling was extended to Penning trapping of heavy ions in high-precision studies of fundamental physical properties [15]. Penning traps rely on a homogeneous magnetic field and quadrupole electric field for axial confinement of ions, and buffer gas cooling is used to reduce the energy of the ion and make it susceptible to trapping. In 2002, the Doyle group at Harvard utilized buffer gas cooling for the first time to cool a Rb atomic beam [16]. Since then, buffer gas cooling has been a preferred method for producing intense, cold, and slow atomic and molecular beams. In the

experiments detailed here, buffer gas cooling is used to cool both atomic beams (Ba) and molecular beams (BaF, CaF).

The process of forming a buffer-gas cooled molecular beam consists of three stages: (i)thermalization, (ii)diffusion, and (iii) extraction. Upon production of the molecule of interest, which can be done by any of a variety of methods (e.g. laser ablation, beam injection, capillary filling), the molecules will thermalize to the temperature of the buffer gas, given certain conditions dependent on the buffer gas flow rate and the dimensions of the cell. The first requirement is that the thermalization distance of the molecule does not exceed the cell length. It is crucial that a molecule of interest experiences a sufficient number of collisions with buffer gas molecules such that it thermalizes to the low temperature of the buffer gas. The molecule's thermalization time can be expressed as $\tau_{therm} = \frac{N\lambda}{v_{cooling}}$, where N is the buffer gas density in the source, λ is the mean free path of the molecule of interest, and $v_{cooling}$ is the average molecular velocity during the thermalization, and has been found to be on the order of several milliseconds.

The second stage, diffusion, is a competition between diffusion to the walls of the chamber and entrainment in a molecular beam via exit through the aperture. For a gas mixture with a small fraction of seeded molecules of interest and a choice of light buffer gas relative to the molecule of interest, the diffusion constant, D, can be given by: $D = \frac{3\pi}{32}\frac{\bar{v}}{n_b\sigma_{b-s}}$ where n_b is the buffer gas density, σ_{b-s} is the elastic collisional cross-section between the buffer gas and the molecule of interest, and $\overline{v_b}$ is the mean buffer gas velocity. From the approximate value for D, the thermal diffusion time is found to be: $\tau_{diff} = \frac{16}{9\pi}\frac{A_{cell}n_b\sigma_{b-s}}{\overline{v_b}}$, where A_{cell} is the aperture area, and, as for the thermalization time, it is on the order of several milliseconds. It has been shown that the linear relationship between the diffusion time and the buffer gas density is applicable only for low buffer gas densities ($\lesssim 3 \times 10^{15} cm^{-3}$) at cold temperatures ($\lesssim$ 20K). [17]

The final step in beam formation is the extraction of the molecules of interest through the aperture of the chamber. The extraction time, $\tau_{extract}$, is related to the cell dimensions by the equation $\tau_{extract} = \frac{4V_{cell}}{\overline{v_b}A_{cell}}$ and is also usually on the order of

	Effusive Oven	Supersonic jet	Buffer Gas
Beam Velocity	200-800 m/s	500-2000 m/s	150-200 m/s
Translational Temperature	500-2000 K	1-5 K	1-5 K
Rotational Temperature	500-2000 K	1-5 K	1-5 K
Particles/Pulse	CW	$\sim 10^{10}$	$> 10^{12}$
Number Density (cm^{-3})	$\sim 10^{6}$	$\sim 10^{5}$	$> 10^{8}$
Number Density/State (cm^{-3})	$\sim 10^{3}$	$\sim 10^{4}$	$\sim 10^{7}$
Shot-to-Shot Stability	$\sim 95\%$	$\sim 50\%$	$\sim 90\%$
Transient broadening	50 kHz	100 kHz	20 kHz
Doppler broadening	200 kHz	200 kHz	20 kHz

Figure 1-3: A comparison of beam properties between beams produced by effusive oven, supersonic jet, or buffer gas. [18]

milliseconds. Efficient pumping of the molecular beam out of the source chamber can be quantified by η_{cell}, definted as the ratio of diffusion time to extraction time,

$$\eta_{cell} \equiv \frac{\tau_{diff}}{\tau_{extract}} \approx \frac{\sigma_{b-s} f_b}{L_{cell} \overline{v_b}}$$

where f_b is the buffer gas flow rate, and L_{cell} is the cell length. η_{cell} is determined by the relative speeds with which a molecule either diffuses to the wall of the source chamber or is extracted through the aperture. When $\eta_{cell} \gtrsim 1$, the extraction times of molecules are shorter than their diffusion times and as a result, efficient pumping out of the source cell is observed. The pumping efficiency increases linearly as η_{cell} increases, eventually plateauing at an upper bound. [4]

Compared to molecular beams prepared by other techniques, buffer gas cooled beams have much slower laboratory frame translational velocities than supersonic beams while having significantly lower center of mass frame translational temperatures than effusive beams. As mentioned before, because the transverse velocity spreads of molecular beams have been shown to increase with increasing Reynolds number of the gas flow, laser interrogation of the beam perpendicular to the beam's translational axis sees less broadening for slower lab frame molecular beams. Thus, the narrower lab frame translational velocity spread results in less Doppler broadening of the molecular spectra, and also increases the interrogation time of the molecular

beam. These experimental advantages make the use of a buffer gas cooled molecular beam source an attractive option compared to effusive or supersonic alternatives.

1.2 Rydberg States of Atoms & Molecules

With regard to this thesis, the ultimate goal of forming intense, cool, and slow atomic and molecular beams is to increase number density in Rydberg states of atoms and molecules. A Rydberg state is an electronically excited state where the electron can be described by high values of the principal quantum number, n. The Rydberg formula: $E = -\frac{\mathcal{R}}{(n-\delta)^2}$ describes the energy of a Rydberg state as a function of n, for quantum defect δ, where $\mathcal{R}$ is the Rydberg constant. The quantum defect, δ, enters due to the interactions of the Rydberg electron with the internal structure of the ion-core for species which are not hydrogen, and leads to the definition of an effective principal quantum number, n*=n-δ [19].

For molecules, the non-spherical, multi-atomic nature of the ion-core affects the electronic structure of the molecule and hence the transition energies between Rydberg states. By probing those Rydberg-Rydberg transitions, electric properties of the ion-core (e.g. multipole moments, polarizability) can be determined. The elliptical orbit of the Rydberg electron around the ion-core for low angular momentum states can result in penetration into the ion-core, reducing the effectiveness of the Rydberg electron as a passive probe of ionic properties. Overcoming this obstacle requires the production of core non-penetrating states, states with higher angular momentum having a larger centrifugal barrier, which scales as $\ell(\ell+1)$.

1.3 Chirped Pulse Millimeter Wave Spectroscopy

For molecules in low-lying electronic states, millimeter waves can be used to probe rotational transitions. However, in the regime of Rydberg states of diatomic molecules' studied here (n*$\approx 35-40$), the energy separation between electronic levels ($= \frac{2\mathcal{R}}{n*^3}$) for $\Delta n^* = 1$, where n^* is the effective principal quantum number) also amounts to

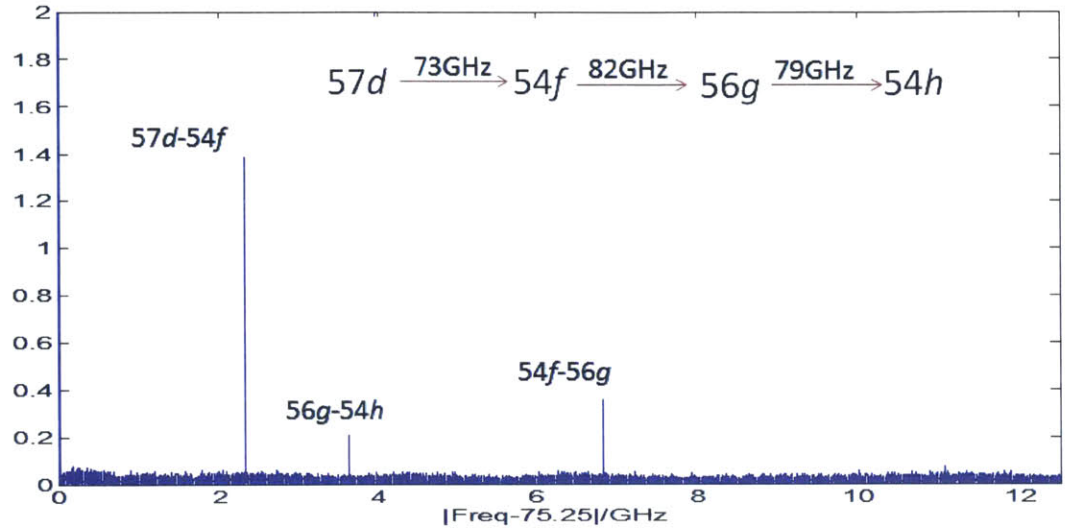

Figure 1-4: A pulse sequence chirped pulse experiment on Rydberg-Rydberg transitions of BaF.

frequencies in the range of millimeter waves (f=70 – 110GHz). Compared to optical transitions, which have a maximal dipole moment of $\approx$ 10 Debye, Rydberg-Rydberg transitions, which can be excited by millimeter waves, can have kiloDebye electric dipole transition moments [20]. A primary challenge in utilizing the advantage of large transition dipole moments has been to achieve sufficiently high frequency resolution (on the order of tens of kilohertz) in a reasonable experimental time.

The Chirped Pulse Fourier Transform Microwave (CP-FTMW) technique was introduced by the Brooks Pate group in 2006 to overcome this obstacle by utilizing a sweep over a broad range of frequencies in a short time interval [21]. By upconverting a frequency chirp, the frequency bandwidth of the chirp is expanded to span a much larger region. This chirp range is used to polarize transitions between the molecular Rydberg states, producing a free induction decay (FID) as the polarization relaxes. A Fourier transform of the resulting FID radiation produced by molecular relaxation yields an emission spectrum that is collected in the time domain and then Fourier-transformed to the frequency domain. Millimeter wave FIDs provide very high resolution Fourier-transformed frequency spectra with resolution to <50kHz. Combining buffer gas cooling with chirped pulse millimeter wave spectroscopy pro-

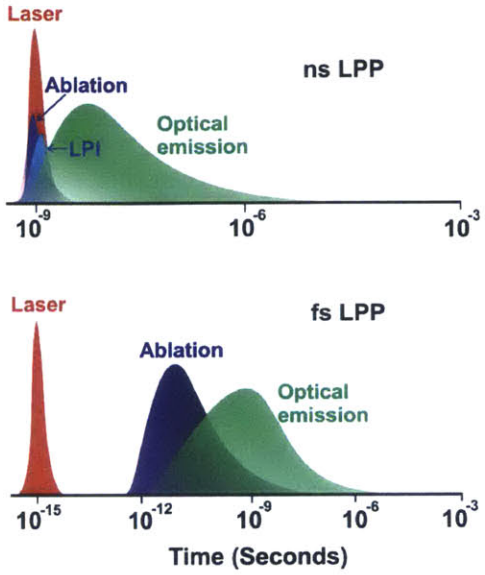

Figure 1-5: In nanosecond laser produced plasma (LPP), the pulse length is sufficiently long that the pulse overlaps temporarily with the plasma from the ablation, leading to laser↔ plasma interactions (LPI). This does not occur with femtosecond pulsed LPP because the laser pulse has terminated well before ablation has begun. [22]

vides the necessary resolution to perform broadband studies of Rydberg states of cold molecules.

As a proof-of-concept, the millimeter wave spectrum presented here shows the production of core non-penetrating states in Ca by sequential excitation up the ladder of orbital angular momentum using a sequence of millimeter wave transitions.

1.4 Laser Ablation

Several years after the invention of the laser around 1960, laser ablation was realized to be a versatile tool to eject material from a solid into the gas-phase [23]. Although much of today's research into laser ablation relates to its usefulness in the precision processing of materials, in this section, only the topic of using laser ablation as a molecular production method will be discussed [24].

In laser ablation of a solid material, the solid-state attractive interactions of the target are overcome by an intense laser pulse and a hot plasma of the material is

produced. The mechanism of ablation is extremely complex and is not well understood. The advantage of laser ablation over other molecular production techniques for gas-phase spectroscopy is its ability to transfer a molecule of interest from the solid phase to the gas phase. Although the resulting gas-phase molecule is initially extremely hot upon production, with several papers having found the initial temperature of the ablation plasma to be >10,000K, this temperature decreases rapidly due to the adiabatic expansion of the plasma plume [22]. The maximum ablation yield, a measure of how much material can be ejected into the gas-phase for a single laser pulse, is target-specific and is determined by the lattice energy of the crystal and the duration and intensity of the laser pulse [25]. An interesting property of laser ablation is that irrespective of the laser's angle of incidence on the target, the produced plasma expands preferentially perpendicular to the ablation target [26].

The quantity and composition of material removal using a high-power laser pulse is strongly dependent on the laser pulse duration and intensity. When using a nanosecond pulsed laser for ablation, the laser pulse melts the surface layer of the ablation target, resulting in transfer of material to both liquid- and gas-phase [27]. Because the plasma is formed before the termination of the laser pulse, there is a resulting laser $\leftrightarrow$ plasma interaction(LPI) between the plasma already formed and the continuing laser pulse. This interaction is reduced when using picosecond or femtosecond laser pulses as ejection of the plasma from the surface occurs after the end of the pulse. The result of LPI is heating of the plasma, and has been shown to produce a larger fractional yield of ionic species compared to shorter pulses which produce predominantly neutral species [22].

Chapter 2

Experimental Design

2.1 Buffer Gas Cooling Apparatus

The buffer gas cooling apparatus was designed by Dr. Yan Zhou and David Grimes for its use in high resolution CPmmW spectroscopy, and is affectionately termed "Buffy". The apparatus can be divided into two main parts: the source chamber and the detection chamber.

The dimensions of the source chamber are 18"x12"x12" and its interior is accessible from four of its six sides. The two-stage Cryomech closed cycle helium refrigerator sits atop the source chamber with the twin tubes of the refrigerator head passing down into the source chamber. Inside of the source chamber is the stainless steel radiation shield of dimensions 11"x7"x7", which is cooled by the first stage of the cryocooler to 40K. Within the radiation chamber, the cold plate is attached to the bottom of the refrigerator head and is cooled by the second stage of the cryocooler to around 20K. The cold cell is mounted to the bottom of the cold plate with the laser ablation target and buffer gas inlet on the backside and the windows for optical input on the front. There is also a smaller optical port for additional probe lasers. Resistive heaters and diode sensors are placed on the cold cell, cold plate, and gas tube to record and control the temperature on all surfaces within the radiation shield.

The detection chamber is separated from the source chamber by a several inch-wide aperture for passage through which the molecular beam passes. The detection

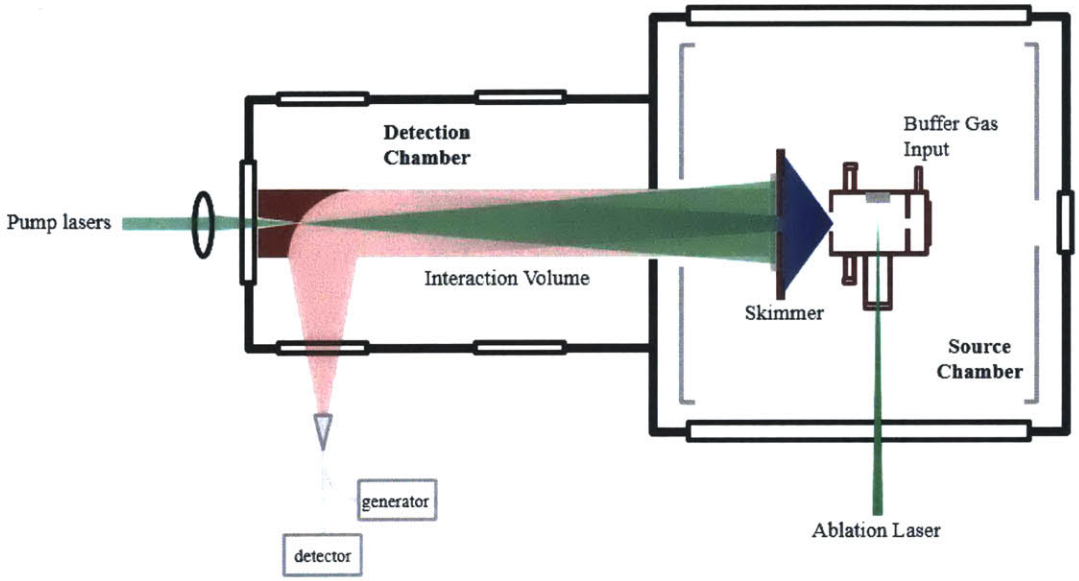

Figure 2-1: The buffer gas cooling apparatus.

chamber features two pairs of windows on either side, constructed of glass or Teflon, for probing by either laser or millimeter waves, respectively. On the inside of the detection chamber is a parabolic mirror for mm-waves, with a central hole drilled out to facilitate overlap with the pump lasers. This experimental setup is used for on-axis experiments that require large interaction volumes.

The key components of the construction to be discussed in this thesis are the laser ablation system of the apparatus, the temperature control loop, and the data acquisition software.

2.1.1 Laser Ablation System

Pellet Production Technique

The source chamber of the apparatus is designed for use with a circular ablation target 0.65" in diameter. The pellet is clamped against the outside of the chamber with four screws and a copper cover. To produce pellets of this size, a die press was machined by the MIT Central Machine Shop with the same diameter.

Pellet production consists of grinding approximately 3-4g of material with mortar and pestle, to be loaded into the die. For BaF_2 pellets, different combinations of BaF_2

and CaF_2 were used in pellet production. The die is pressed using a hydraulic press under 10-15 tons of pressure for between five and thirty minutes. The pellet is then heat-treated in a small vacuum oven by cycling up to 1000°C and then cooling to room temperature three separate times. Heat treatment leads to apparent crystallization and significant increase of the pellet's durability. Upon heat treatment of the barium fluoride, grey and black specks could be seen in the pellet. The impurities were observed exclusively in heat-treated pellets, caused most probably by reaction with water at high temperatures:

$$BaF_2 + 2H_2O \rightarrow Ba(OH)_2 + 2HF$$

Attempts were made to eliminate traces of H_2O from the BaF_2 pellet, including storing the pellets in a dessicator and using 99.99% anhydrous BaF_2. Pellets formed using the anhydrous barium fluoride did not hold up as well as those made using lab-grade BaF_2. Addition of small amounts of CaF_2 (<5% by mass) proved to increase pellet cohesion. Eventually, pellet production was done with pure BaF_2 in order to remove any presence of calcium compounds in the molecular beam. Pressing for ten minutes at twelve tons of pressure produced sufficiently cohesive pellets and heat treatment as described above contributed to the pellet's usability. Pellets of this type were produced up to 4.8g in size, lasting for tens of hours of ablation without fragmenting. This procedure for producing pellets has yielded the greatest signal in spectroscopic experiments, indicating optimal pellet ablation conditions.

Programmatic Laser Ablation

In order to ensure uniform ablation of the pellet target, a programmatic raster scan of laser optics over the surface of the target was implemented. Homogeneous ejection of ablated material is important to maintain a constant number density of the molecule of interest entrained in the buffer gas. This can be best be achieved by moving the ablation spot in order to minimize surface effects.

The experimental setup utilizes a Newport motorized picomotor mirror mount

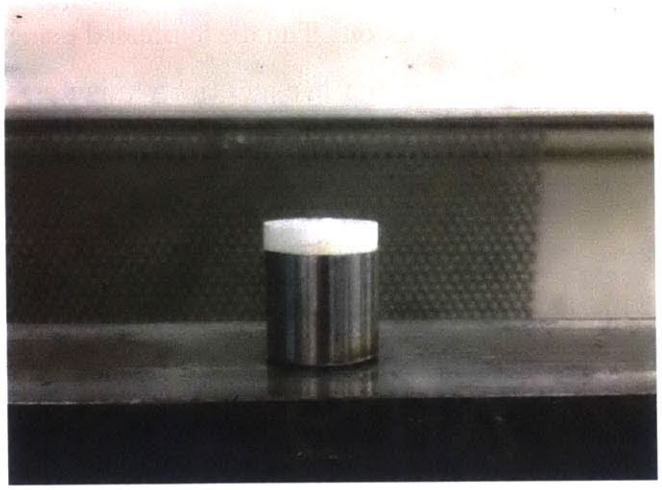

Figure 2-2: A BaF pellet resting on top of its die.

with attached potentiometers in order to tune the motion of the laser spot at a controlled frequency. The mirror steps in one direction while a gating mirror scans the other direction. These are controlled by LabVIEW software developed for this application and integrated with the temperature stabilization loop.

2.1.2 Temperature Stabilization Loop

The radiation plate, source chamber, and skimmer are all cooled using a liquid helium cryostat in order to maintain sufficiently low temperatures to cool the molecular beam efficiently. However, pumping the cryostat cannot be controlled accurately enough to maintain in-chamber temperatures of $<$1K accuracy. To achieve temperature control on that order, resistive heaters and diode sensors are placed on all of the important in-chamber surfaces as parts of a iterative feedback PID loop. The radiation plate is held at 40K by the first stage of the cryostat whereas the source chamber and gas inlet are cooled to 20K using the second chamber of the cryostat. Because neon gas condenses at 20K, this is a lower bound for the cooling of the source of chamber. A LabVIEW program allows the user to set the desired temperatures for each of these surfaces by changing the voltage passed through the resistor from 0 to 8.8V, as well as to monitor the diode sensor outputs.

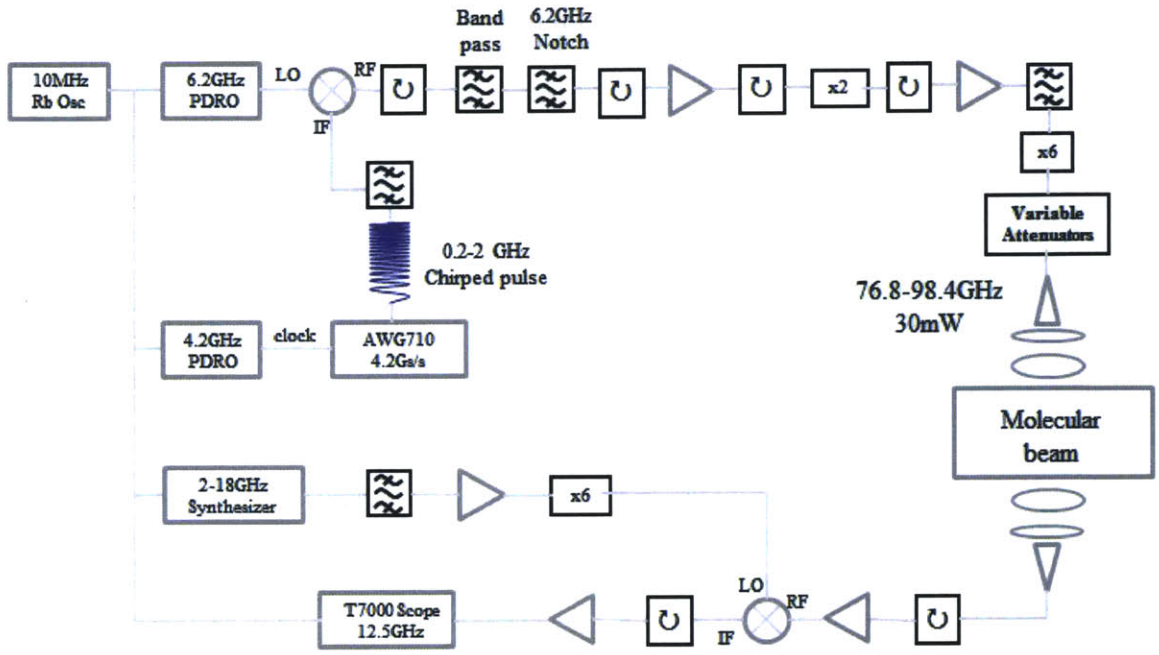

Figure 2-3: The microwave setup used for CPmmW spectroscopy in the buffer gas cooling apparatus.

2.2 Millimeter Wave Setup

The millimeter wave setup begins with a 4.2GS/s Tektronix 710 Arbitrary Waveform Generator capable of outputting frequencies of 0.2-2.0GHz. It is clocked with a 4.2GHz phase-locked dielectric resonator oscillator (PDRO). The chirped signal is passed through a filter and then mixed with a 6.2GHz PDRO. This chirp then passes through a frequency bandpass filter and a 6.1-6.3GHz notch filter to remove all harmonics of the mixing signal and also remove the lower frequency mixed signal. After passing through an isolator, the chirp is upconverted by a factor of twelve, using 2x and 6x active multipliers in succession. The chirped pulse, now spanning the range of 76.8-98.4GHz, can be variably attenuated and is transmitted into the molecular beam through a horn. The FID signal is then collected by the same horn or by a receiving horn placed on the opposite side of the detection chamber of the buffer gas apparatus. It is then downconverted by a 6x multiplied synthesizer frequency ($\approx$ 14.4GHz) and read out on a 12.5GHz Tektronix 700 oscilloscope. All controls of this experiment are

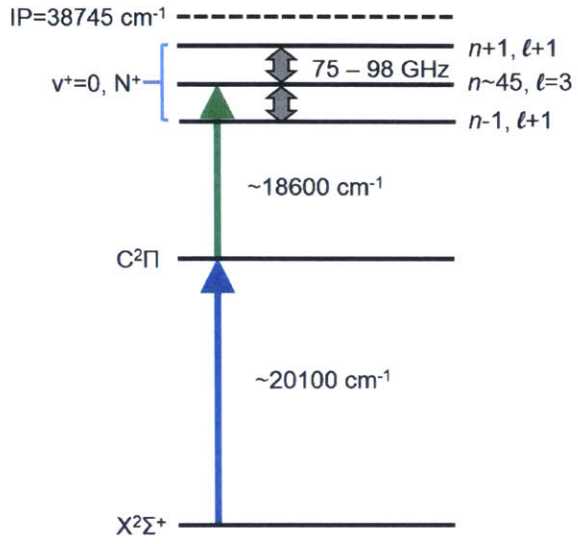

Figure 2-4: Laser and mm-wave excitation scheme for BaF. [18]

done through LabVIEW as discussed below.

The excitation scheme shown in Figure 2-4 displays how the millimeter waves are used to induce Rydberg-Rydberg transitions for n≈45 in BaF. Two pump lasers excite the BaF molecular beam while it is overlapped with the chirped pulse millimeter waves in a large interaction volume. In previous experiments, signal was acquired through a two laser-excitation scheme with an ionization voltage applied to the molecule in the Rydberg state. That scheme offered significantly lower resolution of the Rydberg electronic structure compared to the CPmmW technique.

2.2.1 Data Acquisition

The enhanced LabVIEW data collection program provides a single user interface for entire experimental control. The program is an adaptation of previous software written for the GERTRUDE apparatus, including additional features necessary for the microwave component of the experiment. Program capabilities include setting probe laser scan ranges, data file save locations, peak integration gates, Stark plate voltages, and downconversion frequencies . Eliminating the need for external manual manipulation of these parameters reduces researcher experiment time to only setup

of the scan. The user interface also grabs spectral data displayed on the digital oscilloscope, and displays wavemeter readings for all frequency steps. This allows the researcher to consult a single screen for all updated parameters of the scan. The program saves the input parameters, FID spectra, and wavemeter readings for every scan to the file location specified by the user.

Downconversion of the FID signal results in positive and negative combinations with the mixing frequency, so two separate synthesizer frequencies must be used in order to determine which combination the downconversion represents. In addition, becase the microwaves can stimulate either absorptive or emissive transitions, the FID's phase profile must be evaluated to determine whether an upward or downward transition took place.

2.3 Laser Ablation Studies

Nanosecond-pulsed ablation studies of the ratio of ionic to neutral components of the plasma are undertaken for both Ca and Ba targets. These studies are conducted under a flow of neon gas into the source chamber, such that the atomic and ionic composition determined by the ablation study will be representative of their compositions in the formation of an atomic beam. An Ocean Optics UV-Vis spectrometer is mounted to a window of the source chamber of the buffer gas cooling apparatus using a six inch lens tube to remove background light. The emission spectra for the plasma is collected for different laser fluences, altered by changing the Q switch delay time of the ablation Nd:YAG.

Chapter 3

Results & Discussion

Construction of the buffer gas cooling apparatus with application to Rydberg spectroscopy is the primary focus of this thesis. In this section, the results of experiments conducted to characterize the effectiveness of the apparatus to properly cool both atomic and molecular beams are presented. In addition, the initial mm-wave experiments conducted in the beam are presented, along with an additional section on the effects of laser fluence on ablation in the chamber.

3.1 Experimental Design Diagnostics

To determine the rotational temperature of the molecular beam, laser induced fluorescence experiments for both barium monofluoride and calcium monofluoride were performed in the buffer gas cooling apparatus. The LIF spectra were then fitted to PGopher simulated spectra in order to match the relative intensities of the experimental spectra to a simulation temperature [28]. For BaF, the rotational temperature was found to be 10K; for CaF, the rotational temperature was calculated to be 7K. Assuming that the cross section for cooling translational degrees of freedom is of the same order as cooling rotational degrees of freedom, the assumption can be made that the translational temperatures are of this magnitude, if not colder. Cooling to below the temperature of the buffer gas results from isentropic expansion of the molecular beam out of the source cell. These spectra provide good agreement with the source

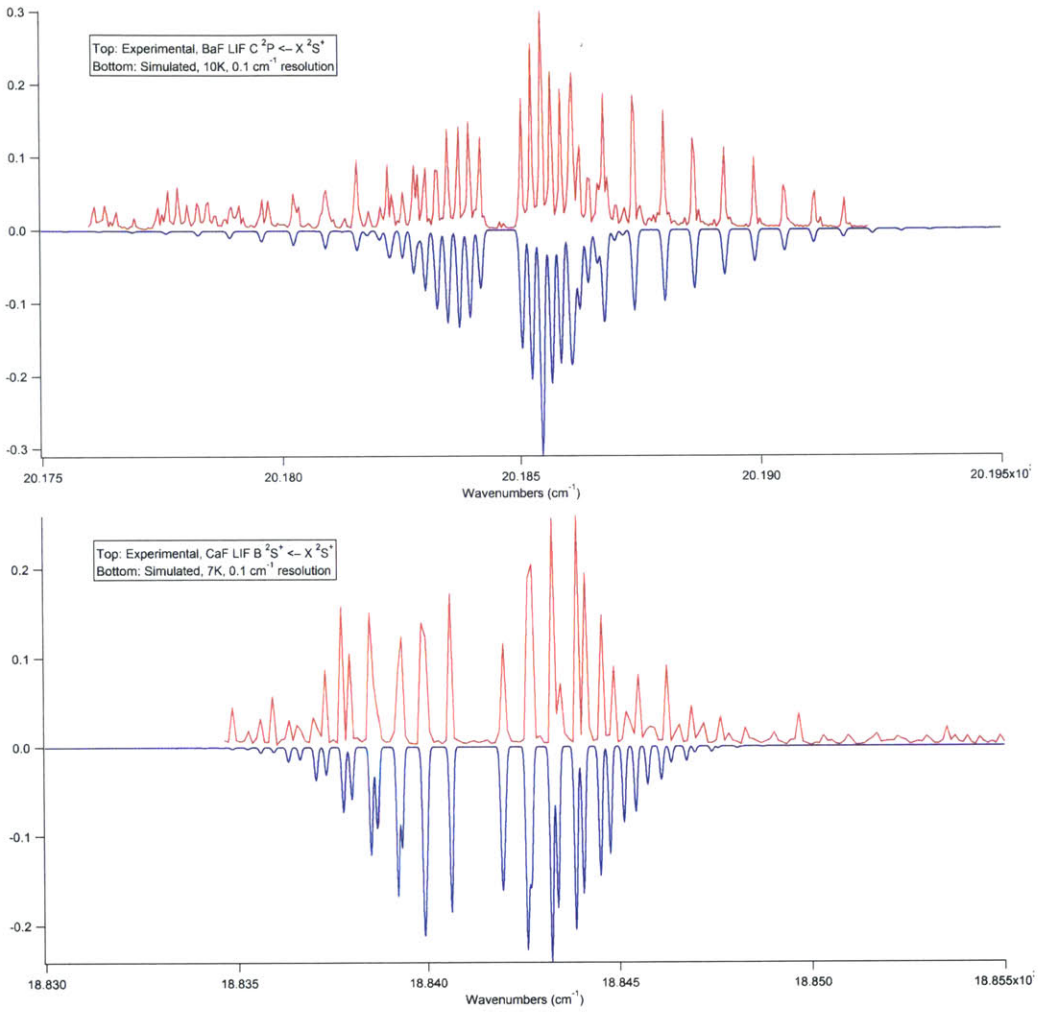

Figure 3-1: LIF spectra of BaF(top) and CaF(bottom) matched with PGopher simulation spectra. The BaF spectral intensities match simulated spectra at 10K and the CaF spectra matches simulations at 7K.

chamber temperatures recorded using the attached diode sensors, and confirm the cooling effects of the buffer gas on the molecular beam.

The number density of BaF in the molecular beam was also determined from the LIF spectral intensity. The total number density was quantified as $10^8/cm^3$ whereas the number density per quantum state was on the order of $10^7/cm^3$. These values were calculated using LIF intensities, the detector's solid angle and quantum yield, as well as the bias voltage on the photomultiplier tube. The fractional population transfer to the excited state and the fluorescence lifetime were also needed. The

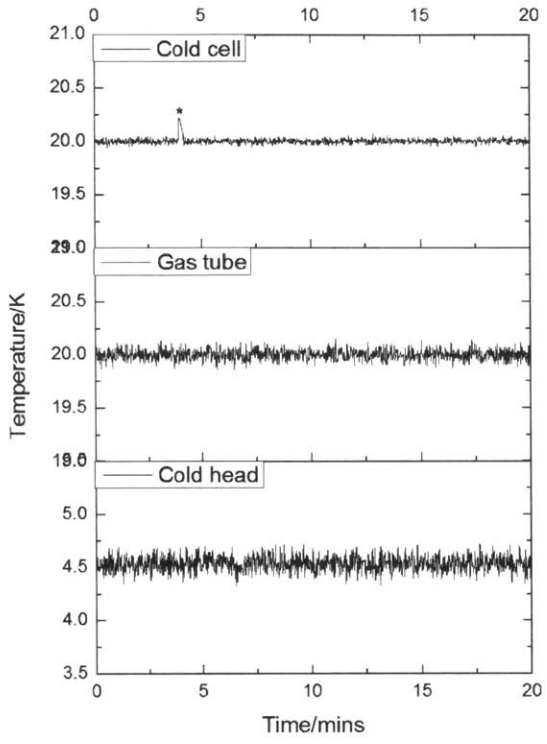

Figure 3-2: Temperature stability of the cold cell, gas tube, and cold head are shown over a period of 20 minutes to be within ±0.25K. The peak in cold cell temperature is due to an ablation laser pulse.

primary uncertainty in the measurement is due to to uncertainty in the probe laser power.

Additional experiments have been started to utilize absorption spectroscopy with a CW infrared laser to quantify the buffer gas cooling and molecular beam properties, such as thermalization time, vibrational and rotational temperatures, ablation yield, and extraction efficiency. These experiments utilize the A $\leftarrow$ X transition in BaF and measure both the dependence of the absorption on delay from the ablation laser as well as rotational and vibrational populations to determine these properties. Similar diagnostic experiments have been performed by the DeMille group at Yale on a buffer gas cooled beam of SrF [29].

The temperatures of the cold cell, gas tube (Ne inlet), and cold head are shown for the buffer gas cooling apparatus in Figure 3-2. Temperature stability of ±0.25K

is seen for all internal source chamber surfaces for arbitrarily long periods of time. The transient feature seen in the cold cell temperature corresponds to the firing of the ablation laser into the cell.

3.2 Millimeter Wave Spectra

Experiments using the on-axis millimeter wave setup, as discussed in section 2.1, show a Doppler shifted doublet due to the co-propagation and counter-propagation of the chirped pulse millimeter wave with the molecular beam. The spectrum in Figure 3-3 shows the 42p-40d transition in Ba atoms averaged over 1000 pulses. The spectral linewidth is observed to be only 75kHz,which illustrates the advantage of measuring the FID signal of a Rydberg transition instead of the signal due to ionization from a Rydberg state. The FID signal resolution is blackbody limited at ≈50kHz. Residual linewidth is due to the presence of collective effects (e.g. superradiance). The Doppler shift between the peaks of the doublet is used as a measure of the laboratory frame translational velocity of the molecular beam. For a splitting of 150kHz, the corresponding lab frame translational velocity of the Ba atomic beam is 200m/s, a factor of three less than that of a beam undergoing supersonic expansion using argon as the carrier gas.

Chirped pulse millimeter wave experiments on BaF molecular beams have also been performed in the buffer gas cooling apparatus, although assignment of those spectral lines have not yet been made.

3.3 Laser Ablation Studies

The intensities of atomic and ionic transitions in ablated Ca and Ba are plotted as functions of laser fluence in the below figures. For Ba(I) (Ba atom), the intensity displayed is that of the $6s^2(^1S) \leftarrow 6s6p(^1P_0)$ transition at 552.756 nm, while for Ba(II) (Ba ion) the transition used is $6s(^2S_{1/2}) \leftarrow 6p(^2P^0_{1/2})$ occurring at 493.41nm. For Ca(I), the 616.217 nm $3p^64s4p(^3P^0_2) \leftarrow 3p^64s5s(^3S)$ transition was used and for

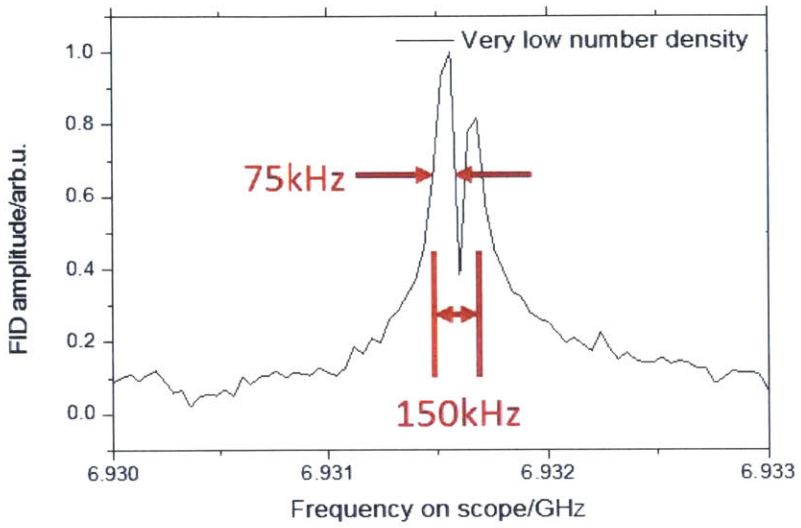

Figure 3-3: A Doppler doublet of Ba atom observed with the on-axis CPmmW setup in the buffer gas cooling apparatus. Doppler broadening gives a laboratory frame forward velocity of 200m/s.

Ca(II), the transition $3p^6 3d(^2D_{5/2}) \leftarrow 3p^6 4p(^2P^0)$ at 854.209 nm was used. The spectrometer is only accurate to $\pm$1nm and the frequencies recorded here match the NIST recorded transition energies to within uncertainty [30]. Previous literature has also utilized the Ba(I) and Ba(II) transitions used here as representative of the two species, whereas different transitions were chosen for characterizing the intensities of Ca(I) and Ca(II).

Previous studies of the ablation of barium and calcium, among other metals, shows a sigmoidal relationship between the spectral intensity of the plasma emissions and the laser fluence [31]. This sigmoidal relationship is a function of the material ejected via ablation, M_J:

$$M_J(\phi) = A_2(\phi) + \frac{A_1(\phi) - A_2(\phi)}{1 + (\frac{\phi}{\phi_c})^{S_C}}$$

where ϕ is the laser fluence in J/cm^2, A_1 is the bound on ablated material for low ϕ, A_2 is the bound on ablated material for high ϕ, ϕ_C is the critical fluence (the fluence at which ablation becomes the dominant material process), and S_C is a surface-dependent parameter. The sigmoidal fit can be broken up into three regions: Arrhe-

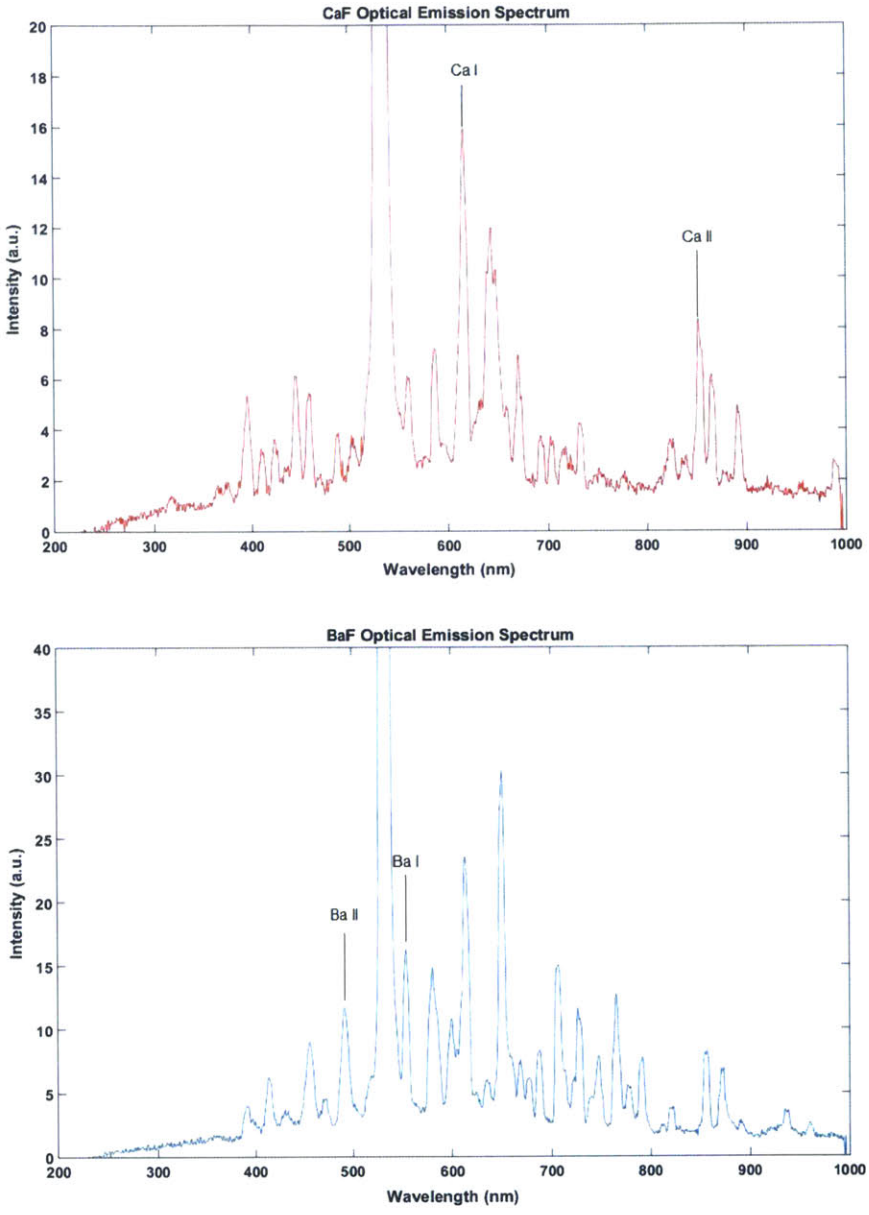

Figure 3-4: Optical emission spectra of CaF and BaF.

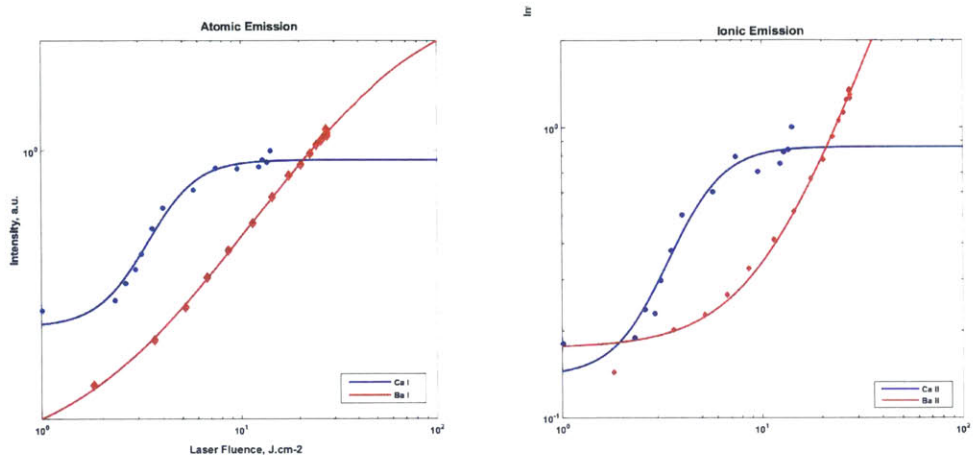

Figure 3-5: Atomic and ionic emission intensities for Ca and Ba as a function of laser fluence. Note: The reported laser fluences are an order of magnitude smaller than as represented in this figure.

nius, Linear, and Beer-Lambert. In the Arrhenius region, $A_1(\phi) \propto \exp(\frac{-\Delta H}{\phi})$ where ΔH is the vaporization energy of the ablation target material. In the Beer-Lambert region $A_2(\phi) \propto \ln[\frac{\phi}{\phi_{th}}]$, where ϕ_{th} is the threshold fluence. Where these two regions converge is the linear region where $M_J(\phi) \propto \phi$. Fluence was calculated by measuring laser power for a 532nm YAG operating at a 10Hz repetition rate and assuming a spot size of 0.1cm^2.

Sigmoidal fitting of the calcium atom and ion data gave R^2 values of >0.99 with all three regimes (Arrhenius, linear, Beer-Lambert) for the observed range of laser fluence. The experimental critical fluence values determined by the sigmoidal fit for Ca was 0.40J/cm^2, which agrees within an order of magnitude with a literature value of 4.4J/cm^2, which was obtained using a 1064nm Nd:YAG for ablation. In order to determine whether the difference between these values is a function of the ablation pulse wavelength or another property, measurement of the laser ablation spot size is required, as well as more sensitive power measurements. The experimental S_C value for Ca was 3.56 compared to a literature value of 2.4 ± 0.4. This parameter has been found to have an inverse relationship with the roughness of the target surface, indicating that the Ca target used in this experiment had a smoother surface compared to that in literature [31].

For the barium data, a much more linear fit was observed, possibly indicating that the laser fluences used were not high or low enough to observe the other two regimes. The ablation pulse energy used here is in the range of 1-10mJ whereas that used in previous experiments spanned 5-180mJ. Observing that, unlike the calcium data, both the barium atom and ion emission intensities do not plateau for the used laser fluences, suggests that larger material ejection is possible for experiments using barium atomic beams.

Chapter 4

Conclusions

Diagnostic experiments done on the buffer gas cooling apparatus have shown effective buffer gas cooling of molecular beams of a variety of species. Effective cooling of the source chamber for long periods of time (>10 hours) has been achieved and efficient ablation of different species has been optimized. Translational and rotational temperatures of <10K have been observed, and lab frame translational velocities of 200m/s have been realized. Additional CW absorption spectroscopy experiments must still be conducted to further characterize the molecular beam formation. Use of the buffer gas cooled molecular beam for high-resolution CPmmW spectroscopy has been successful on both atoms (Ba) and molecules (BaF), and will have valuable applications in Rydberg electronic spectroscopy, probing electric properties of the ion-core. Studies of laser ablation in the apparatus have expanded upon results in the literature for different ablation laser wavelength and a different range of laser fluence. A study of the composition resulting from laser ablation of the alkaline earth halides is the next step.

Overall, combining the techniques of buffer gas cooling and chirped pulse microwave spectroscopy have led to orders of magnitude improvement in both the resolution and the reduction of time required to record molecular Rydberg spectra. This has allowed for the observation of molecular Rydberg-Rydberg transitions not previously observable in supersonically expanded beams. Through the increased number density, decreased translational velocities, higher spectral resolution, and shorter experiment

times that this apparatus provides, molecular spectroscopists have a promising new avenue to reap a wealth of information contained in the Rydberg regime.

Bibliography

[1] Donald H Levy. The Spectroscopy of Very Cold Gases. *Science*, 214(4518):263–269, 1981.

[2] J. Deckers and J. B. Fenn. High intensity molecular beam apparatus. *Review of Scientific Instruments*, 34(1):96–100, 1963.

[3] Ellison H. Taylor and Sheldon Datz. Study of chemical reaction mechanisms with molecular beams. the reaction of k with hbr. *The Journal of Chemical Physics*, 23(9), 1955.

[4] NR Hutzler, HI Lu, and JM Doyle. The buffer gas beam: An intense, cold, and slow source for atoms and molecules. *Chemical reviews*, 2012.

[5] Martin Knudsen. Die Molekularströmung der Gase durch Öffnungen und die Effusion. *Annalen der Physik*, 333(5):999–1016, 1909.

[6] Sebastiaan Y. T. van de Meerakker, Hendrick L. Bethlem, and Gerard Meijer. Taming molecular beams. *Nature Physics*, 4(8):595–602, 2008.

[7] David M. Lubman, Charles T. Rettner, and Richard N. Zare. How isolated are molecules in a molecular beam? *The Journal of Physical Chemistry*, 86(7):1129–1135, 1982.

[8] R. F. Code. A Low Temperature Molecular Beam Source. *Review of Scientific Instruments*, 42(6):896, 1971.

[9] Arthur Kantrowitz and Jerry Grey. A high intensity source for the molecular beam. Part I. Theoretical. *Review of Scientific Instruments*, 22(5):328–332, 1951.

[10] E.W. Becker and K. Bier. Dei Erzeugnung eines intensiven, teilweise monochromatisierten Wasserstoff-Molekularstrahles mit einer Laval-Duse. *Zeitschrift Naturforschung Teil A*, 9:975, 1954.

[11] Richard E. Smalley, Lennard Wharton, and Donald H. Levy. Molecular optical spectroscopy with supersonic beams and jets. *Accounts of Chemical Research*, 10(4):139–145, 1977.

[12] D. Williams. *Molecular Physics: Methods of Experimental Physics*. Elsevier Science, 2013.

[13] Nicholas R. Hutzler, Maxwell Parsons, Yulia V. Gurevich, Paul W. Hess, Elizabeth Petrik, Ben Spaun, Amar C. Vutha, David DeMille, Gerald Gabrielse, and John M. Doyle. A cryogenic beam of refractory, chemically reactive molecules with expansion cooling. pages 18976–18985, 2011.

[14] J. K. Messer and Frank C. De Lucia. Measurement of pressure-broadening parameters for the CO-He system at 4 K. *Physical Review Letters*, 53(27):2555–2558, 1984.

[15] G. Savard, St. Becker, G. Bollen, H.-J. Kluge, R.B. Moore, Th. Otto, L. Schweikhard, H. Stolzenberg, and U. Wiess. A new cooling technique for heavy ions in a Penning trap. *Physics Letters A*, 158(5):247–252, 1991.

[16] Dima Egorov, Thierry Lahaye, Wieland Schöllkopf, Bretislav Friedrich, and John Doyle. Buffer-gas cooling of atomic and molecular beams. *Physical Review A*, 66(4):1–8, 2002.

[17] S. M. Skoff, R. J. Hendricks, C. D. J. Sinclair, J. J. Hudson, D. M. Segal, B. E. Sauer, E. A. Hinds, and M. R. Tarbutt. Diffusion, thermalization, and optical pumping of ybf molecules in a cold buffer-gas cell. *Phys. Rev. A*, 83:023418, Feb 2011.

[18] Yan Zhou. *Direct observation of Rydberg-Rydberg transitions via CPmmW spectroscopy.* PhD thesis, Massachusetts Institute of Technology, 2014.

[19] Jeffrey J. Kay, Stephen L. Coy, Bryan M. Wong, Christian Jungen, and Robert W. Field. A quantum defect model for the s, p, d, and f rydberg series of caf. *The Journal of Chemical Physics*, 134(11):–, 2011.

[20] Anthony P. Colombo, Yan Zhou, Kirill Prozument, Stephen L. Coy, and Robert W. Field. Chirped-pulse millimeter-wave spectroscopy: Spectrum, dynamics, and manipulation of rydbergâĂŞrydberg transitions. *The Journal of Chemical Physics*, 138(1):–, 2013.

[21] Gordon G. Brown, Brian C. Dian, Kevin O. Douglass, Scott M. Geyer, and Brooks H. Pate. The rotational spectrum of epifluorohydrin measured by chirped-pulse Fourier transform microwave spectroscopy. *Journal of Molecular Spectroscopy*, 238(2):200–212, 2006.

[22] B. Verhoff, S. S. Harilal, J. R. Freeman, P. K. Diwakar, and a. Hassanein. Dynamics of femto- and nanosecond laser ablation plumes investigated using optical emission spectroscopy. *Journal of Applied Physics*, 112(9), 2012.

[23] John C Miller. A brief history of laser ablation. *AIP Conference Proceedings*, 288(1):619, 1993.

[24] K. Zimmer. Laser Processing and Chemistry, 1999.

[25] M. Villagran-Muiz, H. Sobral, C. a. Rinaldi, I. Cabanillas-Vidosa, and J. C. Ferrero. Optical emission and energy disposal characterization of the laser ablation process of CaF2, BaF2, and NaCl at 1064 nm. *Journal of Applied Physics*, 104(10), 2008.

[26] Tao Wu, Xinbing Wang, Shaoyi Wang, Jian Tang, Peixiang Lu, and Hong Lu. Time and space resolved visible spectroscopic imaging co2 laser produced extreme ultraviolet emitting tin plasmas. *Journal of Applied Physics*, 111(6):–, 2012.

[27] B. N. Chichkov, C. Momma, S. Nolte, F. von Alvensleben, and A. Tunnermann. Femtosecond, picosecond and nanosecond laser ablation of solids. *Applied Physics A: Materials Science & Processing*, 63(2):109–115, 1996.

[28] Timothy C Steimle, Sarah Frey, Anh Le, David Demille, David a Rahmlow, and Colan Linton. Molecular-beam optical Stark and Zeeman study of the A 2 âĂŞ X (0 , 0) band system of BaF. *Physical Review A*, 012508:1–12, 2011.

[29] J F Barry, E S Shuman, and D DeMille. A bright, slow cryogenic molecular beam source for free radicals. *Physical chemistry chemical physics : PCCP*, 13(42):18936–47, November 2011.

[30] A Kramida, Yu Raichenko, J Reader, and NIST ASD Team. NIST Atomic Spectra Database (version 5.2), 2014.

[31] Ivan Cabanillas-Vidosa, Carlos a. Rinaldi, and Juan C. Ferrero. Optical emission and mass spectrometric characterization of laser ablation process of Ca, Mg, and Ba at 1064 nm. *Journal of Applied Physics*, 102(1):013110, 2007.